THE BENARD PROBLEM: A COMPARISON OF FINITE DIFFERENCE AND SPECTRAL COLLOCATION EIGENVALUE SOLUTIONS

J. Raymond Lee Skarda
NASA Lewis Research Center
Cleveland, Ohio

and

Frances E. McCaughan and Nessan Fitzmaurice
Case Western Reserve University
Cleveland, Ohio

Summary

The application of spectral methods, using a Chebyshev collocation scheme, to solve hydrodynamic stability problems is demonstrated on the Benard problem. Implementation of the Chebyshev collocation formulation is described. The performance of the spectral scheme is compared with that of a 2nd order finite difference scheme. An exact solution to the Marangoni-Benard problem is used to evaluate the performance of both schemes. The error of the spectral scheme is at least seven orders of magnitude smaller than finite difference error for a grid resolution of N = 15 (number of points used). The performance of the spectral formulation far exceeded the performance of the finite difference formulation for this problem. The spectral scheme required only slightly more effort to set up than the 2nd order finite difference scheme. This suggests that the spectral scheme may actually be faster to implement than higher order finite difference schemes.

1.0 Introduction

The theory of hydrodynamic stability has helped to explain and predict a variety of fluid flow phenomena. Recently it is being used to guide the modern computational fluid dynamicist in choosing the appropriate parameter values which are needed to simulate fluid flow behavior of interest (NASA TM-4569, 1994). Many current applications of hydrodynamic stability theory are possible because the field has benefitted greatly from the development and refinement of computational tools in addition to the existence of increasingly powerful computers. Spectral methods is one such set of tools that has been successfully applied to obtain high accuracy hydrodynamic stability results to previously intractable problems.

The purpose of this paper is to show, by example, the use of a spectral collocation formulation to solve hydrodynamic stability problems. Our discussion will be confined to the linear stability analysis which is the foundation of hydrodynamic stability theory (Lin, 1945). The linear stability problem ultimately reduces to a matrix eigenvalue problem, and the peril of the eigenvalue problem is that it requires $O(N^3)$ operations to obtain the eigenvalues where the matrix is $N \times N$. As shown herein, the high accuracy of spectral methods results in small N, therefore considerably less CPU time is required to solve for the eigenvalues when compared to finite difference methods.

The Benard problem is used to illustrate the implementation and performance of the spectral scheme. The problem is also solved using a 2nd order finite difference scheme which required slightly less time to implement. Results of the two numerical schemes are compared to the exact solution of the Marangoni-Benard problem (Pearson, 1959).

The Benard problem is described, and the governing equations and boundary conditions are developed in the following section. After a brief description of the finite difference scheme, the spectral collocation formulation is discussed. Results from both numerical schemes are then compared to an exact solution of the Marangoni-Benard problem. The spectral scheme yields results with considerably better accuracy using an order of magnitude less points than the finite difference scheme.

2.0 Description of Benard Problem & Development of Equations

A temperature difference is imposed normal to the free surface of a thin liquid layer of fluid of infinite horizontal extent and finite thickness, d, as shown in Figure 1.The initial steady state or base state of the system is one of no fluid motion, with a linear temperature profile across the layer. The velocity and temperature profiles illustrated in Figure 1 can immediately be expressed as, $U_b^* = 0$ and $T_b^* = T_{b0}^* - \beta z^*$. Using the notation of Pearson (1958) and Chandrasehkar (1981), U_b^* and T_b^* are respectively, the base flow velocity and temperature. The temperature gradient of the base state, β is defined as $\beta = -dT_b^*/dz^*$ or $\beta = \Delta T_d^*/d$ where $\Delta T_d^* = T_{b0}^* - T_{bs}^*$. The asterisk, "*" denotes dimensional quantities. The lower surface is rigid and is held at a constant temperature. The upper surface is free and exchanges heat with the environment . The free surface is assumed flat which is physically justified for many terrestrial problems. We first give the nondimensional form of the governing equations and in the next section we linearize about the base state just described in order to determine whether small disturbances to the base state will grow or decay. Specifically we are interested in the critical values of the nondimensional parameters where the change of stability occurs.

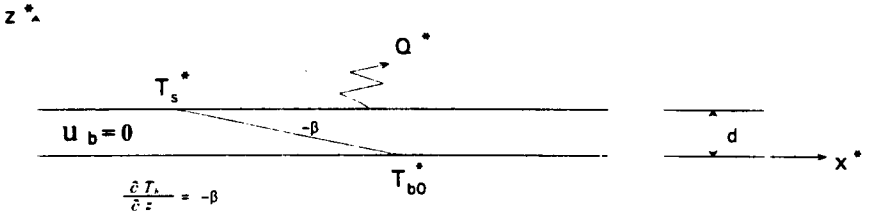

Figure 1 Base State For Thin Liquid Layer Of Infinite Extent

Nondimensional forms of mass, momentum, and energy equations for an incompressible fluid with the Boussinesq approximation are given in equations (1) through (3). The derivation of these equations with the Boussinesq approximation and constant viscosity and their subsequent nondimensionalization are well known and we refer the interested

reader to Chandrasekar (1981), and Drazin & Reid (1982) for details. All thermophysical properties are assumed constant apart from density and surface tension.

$$\bar{\nabla}\cdot\bar{U} = 0 \tag{1}$$

$$\frac{D\bar{U}}{Dt} = -\bar{\nabla}P + \hat{k}\cdot Ra\,Pr(T - T_{b0}) + Pr\,\bar{\nabla}^2\bar{U} \tag{2}$$

$$\frac{DT}{Dt} = \bar{\nabla}^2 T \tag{3}$$

$\bar{U}$, T, P, t are the velocity vector, temperature, pressure, and time respectively. The reference values used to nondimensionalize the variable; length, velocity, temperature, pressure, and time are d, κ_0^*/d, βd, $\rho_0^*\kappa_0^*/d^2$, d^2/κ_0^*, respectively. ρ_0^* is the fluid density and κ_0^* is the fluid thermal diffusivity. The subscript 0 indicates that the properties are chosen at the lower surface temperature, T_{b0}. The characteristic value of the dynamic viscosity of the fluid, μ, is denoted as μ_0^*. These reference values are consistent with those used in the buoyancy instability studies presented in Chandrasekhar (1981) and Drazin and Reid (1982), and the surface tension instability investigations of Pearson (1958) and Scriven and Sternling (1964). Two dimensionless groups appear in the momentum equation, the Prandtl number, Pr, and the Rayleigh number, Ra, which are defined as follows:

$$Pr = \frac{\mu_o}{\rho_0^*\kappa_0^*} \qquad Ra = \frac{\rho_0^*\beta d^4 \xi_0^* g_z}{\kappa_0^*\mu_0^*}.$$

ξ_0^* is the volumetric thermal expansion coefficient and g_Z is gravitational acceleration in the negative z-direction. The dot product of the unit vector in the z direction, $\hat{k}$, and the buoyancy (RaPr) term in equation (2) indicates that buoyancy only acts in the vertical direction. Therefore the Rayleigh number only occurs in the z-momentum equation.

The nondimensional boundary conditions are given by equations (4) and (5). Equations (4a,b,c), represent the no-slip conditions and impenetrable wall condition at z=0. Equation (4d) is the constant temperature condition along the wall. The normal stress boundary condition reduces to (5a) when the free surface at z=1 is assumed to be flat. Boundary condition (5b) is the heat flux balance at the free surface, where Q* is the dimensional surface heat flux to the environment and k_0^* is the fluid thermal conductivity. Equations (5c and 5d) are the tangential force balances along the free surface, in the x and y directions, respectively.

$$\text{At } z = 0; \quad \bar{U}(0) = (U_x, U_y, U_z) = 0, \quad T(0) = T_{b0} \tag{4a,b,c,d}$$

$$\text{At } z = 1; \quad U_z(1) = 0; \quad \frac{\partial T}{\partial z} + \frac{Q^*}{k_0^*\beta} = 0, \tag{5a,b}$$

$$-\left[\left(\frac{\partial U_z}{\partial x} + \frac{\partial U_x}{\partial z}\right)\hat{i} + \left(\frac{\partial U_z}{\partial y} + \frac{\partial U_y}{\partial z}\right)\hat{j}\right] = Ma\nabla_{II} T \tag{5c,d}$$

The operator, ∇_{II}, is the surface gradient defined as $\hat{i}\frac{\partial}{\partial x}+\hat{j}\frac{\partial}{\partial y}$ where, $\hat{i}$ and $\hat{j}$ are unit vectors in the x and y directions respectively. The Marangoni number, Ma, which occurs in equations (5c,d) is defined as: $Ma=\frac{\beta\, d^2\gamma_0^*}{\kappa_0^*\mu_0^*}$. The parameter, γ_0^*, is defined as $-\left.\frac{\partial\sigma^*}{\partial T^*}\right|_{T_{bs}}$, and is often referred to as the temperature variation of surface tension (Nield 1964 and Adamson 1967) or differential coefficient of surface tension change with temperature (Scriven and Sternling 1964). The surface tension, σ^*, does not appear in our equations or boundary conditions since we have assumed a flat interface. Further discussion of the nondimensionalization of the free surface boundary conditions is found in Scriven and Sternling (1964), and Koschmeider (1993).

The surface heat flux, Q^*, has to be expressed in a form that is suitable for linearizing the heat flux boundary condition, equation (5). This is accomplished by expanding Q^* about the base state surface temperature, T_{bs}^*. The first order expansion is given by equation (6). As previously noted, the base state varies only in the z-direction. Therefore, $Q^*(T_{bs})$ can be re-expressed as equation (7), using Fourier's law.

$$Q^* = Q^*(T_{bs}^*)+\left.\frac{\partial Q^*}{\partial T^*}\right|_{T_{bs}^*}\left(T^*-T_{bs}^*\right) \tag{6}$$

$$Q^*\left(T_{bs}^*\right)=k_0^*\left.\frac{\partial T^*}{\partial z^*}\right|_{z^*=d}=k_0^*\beta \tag{7}$$

Substituting equation (6) into equation (5b), using $k_0^*\beta$ in place of $Q^*\left(T_{bs}^*\right)$ and defining $h^*=\left.\frac{\partial Q^*}{\partial T^*}\right|_{T_{bs}^*}$, the heat flux boundary condition becomes:

$$\frac{\partial T}{\partial z}+1+Bi_s\left(T_s-T_{bs}\right)=0 \tag{8}$$

The dimensionless group, Bi_S, is defined as $Bi_s=\frac{h^*d}{k_0^*}$ and is referred to as either the surface Biot number (Pearson, 1958 and Nield, 1964) or the surface Nusselt number (Scriven and Sternling, 1964).

We note that the three-dimensional mass, momentum, and energy equations are given in equations (1-3), yet the boundary conditions are only specified in the z-direction. After linearizing the problem and applying some vector operations, it is shown in the next section, that the governing equations and boundary equations in the x and y directions do not affect the stability of the base state. Equations (1, 2, 3, 4 . and 5a,c,d and 8) make up the system which we will linearize in the next section.

2.1 Linearization of The Governing Equations

The dependent variables are written in terms of the following base flow and perturbation variables: $\bar{U} = \bar{u}, \quad T = T_b + \theta, \quad \Delta P = \Delta P_b + \Delta p$

After substituting for T_b and $\bar{\nabla} T_b$, the disturbance equations become:

$$\frac{\partial \bar{u}}{\partial t} = -\bar{\nabla} p + \hat{k} \cdot Ra\, Pr\, \theta + Pr\, \bar{\nabla}^2 \bar{u} \tag{9}$$

$$\frac{\partial \theta}{\partial t} - u_z = \bar{\nabla}^2 \theta \tag{10}$$

$\hat{k}$ is the unit vector in the z-direction shown in Figure 1. The curl operator is applied twice to the momentum equation, equation (9), which yields equation (11).

$$\frac{\partial \left(\nabla^2 \bar{u}\right)}{\partial t} = \hat{k} \cdot Ra\, Pr\, \bar{\nabla}_{II}^2 \theta + Pr\, \nabla^4 \bar{u} \tag{11}$$

The first curl operation yields the vorticity equation and eliminates the pressure terms. The second curl operation decouples the momentum equations from each other. The x and y momentum equations become uncoupled from the z-momentum and the energy equations. The z-momentum and energy equations remain coupled through the buoyancy term in equation (11), the convective term in equation (10), and the tangential boundary condition (discussed below). Furthermore, the relevant stability parameters, Ma and Ra, do not appear in either the x or y momentum equation or their associated boundary conditions. Given these considerations, equation (11) reduces to the scalar equation in u_z, equation (12).

$$\frac{\partial \left(\nabla^2 u_z\right)}{\partial t} = Ra\, Pr\, \nabla_{II}^2 \theta + Pr\, \nabla^4 u_z \tag{12}$$

The boundary conditions for the perturbed variables associated with equations (10 and 12) are given by equations (13) through (14).

$$\text{At } z = 0, \qquad u_z = 0; \quad \frac{\partial u_z}{\partial z} = 0; \qquad \theta = 0 \tag{13a,b,c}$$

$$\text{At } z = 1, \qquad u_z = 0; \quad \frac{\partial \theta}{\partial z} + Bi_s \theta(1) = 0 \tag{14a,b}$$

$$-\left(\nabla_{II}^2 u_z - \frac{\partial^2 u_z}{\partial z^2}\right) = Ma \nabla_{II}^2 \theta \tag{14c}$$

2.2 Normal Mode Analysis

Since equations (10) and (12) are linear, we assume solutions for u_Z and ϕ are of the form:

$$u_z = w(z)e^{i(\alpha_x x+\alpha_y y)+\lambda t} \quad \text{and} \quad \theta = \phi(z)e^{i(\alpha_x x+\alpha_y y)+\lambda t}$$

α_X and α_Y are the dimensionless wavenumbers in the x and y directions, and λ is the dimensionless frequency. Substituting these into equations (10) and (12) results in the following ordinary differential equations.

$$\lambda\phi(z) - D^2\phi(z) + \alpha^2\phi(z) - w(z) = 0 \tag{15}$$

$$\lambda\left(D^2w - \alpha^2 w(z)\right) = Ra\,Pr\left(D^2\phi - \alpha^2\phi\right) + Pr\left(D^4w - 2\alpha^2D^2w + \alpha^4 w(z)\right) \tag{16}$$

Where $D = \dfrac{d}{dz}$ and $\alpha^2 = \alpha_x^2 + \alpha_y^2$.

The boundary conditions at z = 0 become:

$$w(0) = 0, \quad Dw(0) = 0, \quad \phi(0) = 0. \tag{17a,b,c}$$

At z=1, the flat interface condition, heat flux condition, and tangential stress boundary condition are:

$$w(1) = 0, \quad D\phi(1) + Bi_s\phi(1) = 0, \quad D^2w = -\alpha^2 Ma\,\phi(1) \tag{18a,b,c}$$

Equations (15 through 18) are solved to determine whether the velocity and temperature disturbances grow or decay for given combinations of the relevant parameters. The relevant parameters are Ma, Ra, and α. Our problem is also referred to as a temporally developing flow problem since the disturbance growth or decay is in time. For temporally developing flows, α_X and α_Y are real and the eigenvalue, λ, is complex. If the real part of λ is positive the disturbance grows, if the real part of λ is negative the disturbance decays in time and if λ is zero, the disturbance persists unchanged in time.

3.0 Discrete Formulations

Two discrete formulations will be applied to the Benard problem, a 2nd order finite difference scheme, and a spectral collocation scheme. Irrespective of the discrete formulation the goal is construct a set of linear equations in form of the general eigenvalue problem, Ax = λBx. Once the eigenvalue problem is setup, solution mechanics are identical. If B is cheaply invertible, it usually pays to reduce the problem to a regular eigenvalue problem of the form Cx =λx, where $C = B^{-1}A$. In this study we used standard QR and QZ eigenvalue subroutines from the IMSL library to solve for the eigenvalues.

3.1 2nd Order Finite Difference Scheme

Equations (15 through 18) were discretized using a standard central difference scheme. Boundary conditions result in solving 2N-1 equations for this formulation. The discretized governing equations, equations (19) and (20), were arranged in the form $Az = \lambda Bz$, which is the generalized eigenvalue problem. Coefficients, a through g, and r are constants.

$$a w_{i-2} + b w_{i-1} + c w_i + d w_{i+1} + e w_{i+2} + r\phi_i = \lambda(f w_{i-1} + g w_i + f w_{i+1}) \quad (19)$$

$$f\phi_{i-1} + g\phi_i + f\phi_{i+1} + w_i = \lambda(\phi_i) \quad (20)$$

Here the boundary conditions for Eq (15) are applied only to the i = 0, 1, N-1, N equations and for Eq (16) only to i = 0 and i = N.

B is a nonsingular matrix so it is possible to reduce the system to a regular eigenvalue problem of the form $Cz = B^{-1}A = \lambda z$. Assuming a flat interface ensures that B is a tridiagonal matrix which can efficiently be inverted using a tridiagonal solver. The problem was discretized in terms of one fourth order equation, and one second order equation, which yields A and B matrices of rank 2N+2. Three of the six boundary conditions are Dirichlet boundary conditions which reduce the A and B matrices to rank 2N-1.

3.2 Chebyshev Collocation Spectral Scheme

The key to all spectral techniques lies in the possibility of expanding smooth functions in terms of rapidly converging sums of certain orthogonal basis functions. For example, consider any reasonable function f(x) defined in the domain $-1 \le x \le 1$ (see Canuto et. al. for a precise definition of "reasonable"). The function can be represented as a sum of Chebyshev polynomials, $T_n(x)$, of the form:

$$f(x) = \sum_{n=0}^{\infty} \hat{f}_n T_n(x) \quad (21)$$

The crucial thing is that the sum converges very rapidly if f(x) is smooth so one can truncate it at N terms and accurately represent the function with a minimal set of numbers $\{\hat{f}_n : n = 0,\ldots,N\}$. Such an expansion can be viewed as a very efficient and only slightly lossy compression technique for functions.

Pure spectral methods proceed by expanding the unknowns in terms of truncated sums of certain polynomials having excellent convergence properties (often simple combinations of Chebyshev polynomials that automatically account for any boundary conditions that must be satisfied by the function). The sums are then substituted into the differential equation and the coefficients are picked to minimize the residual. The fundamental quantities of interest in this procedure are the coefficients in the expansions of the dependent variables.

Spectral collocation methods on the other hand, concentrate directly on the physical space representation of the unknowns and as a consequence are more easily understood by the naive user. For example, in a collocation technique our hypothetical function, f(x) is not stored as $\{\hat{f}_n : n = 0,...,N\}$, but instead as $\{f_i \equiv f(x_i) : i = 0,...,N\}$. The exact correspondence between the two representations is maintained by choosing the physical space grid $\{x_i\}$ in an optimal fashion that is related to one of the Gaussian integration formulas. A typical formula of choice for Chebyshev expansions on the domain [-1,1] is the Gauss-Labatto grid, $x_i = \cos(i\pi / N)$. The spectral space and physical space representations can be interchanged with essentially no error (except perhaps for aliasing errors). Moreover, if the expansion is in terms of Chebyshev polynomials or trigonometric functions, the transformations to and from spectral space can be carried out efficiently by using Fourier Transforms (FFT's).

Solving differential equations obviously requires that the derivatives are evaluated. One method of evaluating $\{f'_i \equiv f'(x_i)\}$ is to proceed as

$$f_i \rightarrow \hat{f}_n \rightarrow \hat{f}'_n \rightarrow f'_i$$

That is, one first transforms to spectral space where a derivative is taken rapidly by using some simple properties of the basis functions. The new series produced in this fashion is then transformed back to a physical space representation. In the case of trigonometric or Chebyshev expansions, the procedure is dominated by the FFT's used in the transformations, so the total cost is $O(N \log N)$ operations.

There is a mathematically equivalent approach which uses matrix-vector multiplies to express

$$f'_i = \sum_{j=0}^{N} D_{ij} f_j \qquad (22)$$

where the elements of the derivative matrix D can be found in spectral texts such as Canuto et. al. To evaluate the derivatives on the entire grid using this method will take $O(N^2)$ operations. However, the matrix-vector multiply approach is the only one possible for eigenvalue problems where the aim is to turn the linear differential operator into the equivalent matrix operator on the discrete grid. Thus for example, the continuous equation, $\lambda f = f''$, becomes the discrete equation, $\lambda f = D^2 f$, so that in theory one simply fills and then squares the D matrix before feeding it to a standard matrix eigenvalue . In practice, the greatest programming labor is in the implementation the boundary conditions.

For the Benard problem, it is convenient to define the matrix operator

$$L = D^2 - \alpha^2 I \qquad (23)$$

where I is the identity matrix. The continuous equations, (15) and (16) then become the discrete equations, (24) and (25)

$$\mathrm{Pr}\left(L^2 w - \alpha^2 \mathrm{Ra}\, I\phi_j\right) = \lambda L w \tag{24}$$

$$L\phi + Iw = \lambda I\phi \tag{25}$$

and these equations can be recast into the standard form $Au = \lambda Bu$ given by equation (26).

$$\begin{bmatrix} \mathrm{Pr}\,L^2 & -\alpha^2 \mathrm{Ra}\,\mathrm{Pr}\,I \\ I & L \end{bmatrix} \begin{bmatrix} w \\ \phi \end{bmatrix} = \lambda \begin{bmatrix} L & 0 \\ 0 & I \end{bmatrix} \begin{bmatrix} w \\ \phi \end{bmatrix} \tag{26}$$

This translation of a continuous problem into a discrete one is very natural and can be carried out even more rapidly than the corresponding process for a finite difference scheme. However, this matrix eigenvalue problem as it stands does not take the boundary conditions into account. Most of the coding complexity that is present in spectral techniques (which by nature are global approximations) arises because of the need to implement boundary data (which are local point conditions).

The boundary conditions and governing equation are first mapped from the z variable in the domain [0,1] to x defined on [-1,1] by $x = 2z-1$. The mapped boundary conditions become:

At x = -1 (i=n): $$w_n = \sum_{i=0}^{N} D_{Ni} w_i = \phi_i = 0 \tag{27}$$

At x = +1 (i=0): $$w_0 = \mathrm{Bi}_s \phi_0 + \sum_{i=0}^{N} D_{0i}\phi_i = \alpha^2 \mathrm{Ma}\phi_0 \sum_{i=0}^{N} D_{0i}^2 w_i = 0 \tag{28}$$

We immediately see that $w_0 = w_N = \phi_N = 0$. The remaining equations can be used to simultaneously solve for w_1, w_{N-1}, and ϕ_0 in terms of the other w_i's and ϕ_i's as shown in equation (29). Equations (29) reveal that elements, w_1 and w_{N-1}, are coupled to the ϕ_i's through the last boundary condition in equation (28) while ϕ_0 remains uncoupled from the w_i's.

$$w_1 = \sum_{i=2}^{N-2} c_i w_i + \phi_0, \quad w_{N-1} = \sum_{i=2}^{N-2} d_i w_i + \phi_0, \quad \phi_0 = \sum_{i=1}^{N-1} e_i \phi_i \tag{29}$$

The boundary condition information is used to reduce the rank of the eigenvalue problem which is given by equation (30).

$$\sum_{j=0}^{2N+1} A_{ij} u_j = \lambda \sum_{j=0}^{2N+1} B_{ij} u_j \tag{30}$$

The first N+1 components of the vector u here corresponds to $\{w_i : i = 0,\ldots,N\}$ and the last N+1 components corresponds to $\{\phi_i : i = 0,\ldots,N\}$. Applying the six boundary conditions, we can eliminate the rows corresponding to $w_0, w_1, w_{N-1}, w_N, \phi_0$, and ϕ_N and expand equation (30) as given below.

$$A_{i1}u_1 + A_{iN-1}u_{N-1} + A_{iN+1}u_{N+1} + \sum_{\substack{j=2 \\ j\neq N-1,N,N+1}}^{2N+1} A_{ij}u_j = \lambda\left(B_{i1}u_1 + B_{iN-1}u_{N-1} + B_{iN+1}u_{N+1} + \sum_{\substack{j=2 \\ j\neq N-1,N,N+1}}^{2N+1} B_{ij}u_j \right) \tag{31}$$

where we have already used the data, $u_0 = u_N = u_{2N+1} = 0$ (which corresponds to $w_0 = w_N = \phi_N = 0$). Using the remaining boundary conditions, equations (29), take the form

$$u_1 = \sum_{j=2}^{N-2} c_j u_j = \sum_{\substack{j=2 \\ j\neq N-1,N,N+1}}^{2N} \bar{c}_j u_j, \quad u_{N-1} = \sum_{j=2}^{N-2} d_j u_j = \sum_{\substack{j=2 \\ j\neq N-1,N,N+1}}^{2N} \bar{d}_j u_j,$$
$$u_{N+1} = \sum_{j=1}^{N-1} e_j u_j = \sum_{\substack{j=2 \\ j\neq N-1,N,N+1}}^{2N} \bar{e}_j u_j \tag{32}$$

$$\text{where} \quad \bar{c}_j = \begin{cases} c_j \\ e_{j-N-3} \end{cases} \quad \& \quad \bar{d}_j = \begin{cases} d_j \\ e_{j-N-3} \end{cases} \quad \& \quad \bar{e}_j = \begin{cases} 0 & \text{if } j = 2,\ldots,N-2 \\ e_{j-N-3} & \text{if } j = N+2,\ldots,2N \end{cases} \tag{33}$$

The matrix eigenvalue problem can be rewritten as

$$\sum_{\substack{j=1 \\ j\neq N-1,N,N+1}}^{2N+1} \bar{A}_{ij}u_j = \lambda \sum_{\substack{j=1 \\ j\neq N-1,N,N+1}}^{2N+1} \bar{B}_{ij}u_j \tag{34}$$

where $\bar{A}_{ij} = A_{ij} + A_{i1}\bar{c}_j + A_{iN-1}\bar{d}_j + A_{iN+1}\bar{e}_j$ and $\bar{B}_{ij} = B_{ij} + B_{i1}\bar{c}_j + B_{iN-1}\bar{d}_j + B_{iN+1}\bar{e}_j$. The global matrix problem is finally transformed to a reduced eigenvalue problem $\tilde{A}u = \lambda\tilde{B}u$ where the matrices are $(2N-4)\times(2N-4)$ and all six boundary conditions have been incorporated into the problem.

The principle difficulty in using spectral collocation techniques for solving stability problems is the implementation of derivative boundary conditions. A condition such as $w(1) = 0$ is not a problem as all that is required is the reduction of the global matrices by eliminating one row and one column. Derivative data on the other hand, results in altering all the elements of the matrices due to the global nature of the underlying series

approximation. All data contributes to the value of the derivative at each point Nevertheless, for the Benard problem, the spectral collocation technique is only slightly more difficult to code than a second order finite difference scheme. As is observed in the subsequent results, the additional coding effort is amply rewarded.

4.0 Results

Under certain conditions, exact solutions to equations (15) through (18) have been obtained. Pearson (1958) derived an exact solution to the Marangoni-Benard problem (Ra = 0) for the case of neutral stability, $\lambda = 0$. His solution reduces to equation (35) for an insulated free surface, Bi = 0. The critical value of the Marangoni number, equation (35), versus the wavenumber is shown in Fig. 3 and is referred to as a neutral stability curve since $\lambda = 0$ for all points along the curve. For values of Ma above this curve are unstable since infinitesimal disturbances. Our objective is to use the above exact result to investigate the accuracy of the aforementioned discrete formulations, so we do not consider alternative exact or approximate solutions which exist for the general problem. The physical interpretation of these results in addition to results from other exact or approximate solutions to the Benard problem are discussed in Pearson 1958, Scriven & Sternling 1964, Smith 1966, Chandrasekhar 1981, and most of the other references cited in section 6.0. We now compare the numerical results to the exact solution.

$$Ma_c = \frac{8\alpha^2 \cosh(\alpha)(\alpha - \sinh(\alpha)\cosh(\alpha))}{\alpha^3 \cosh(\alpha) - \sinh^3(\alpha)} \tag{35}$$

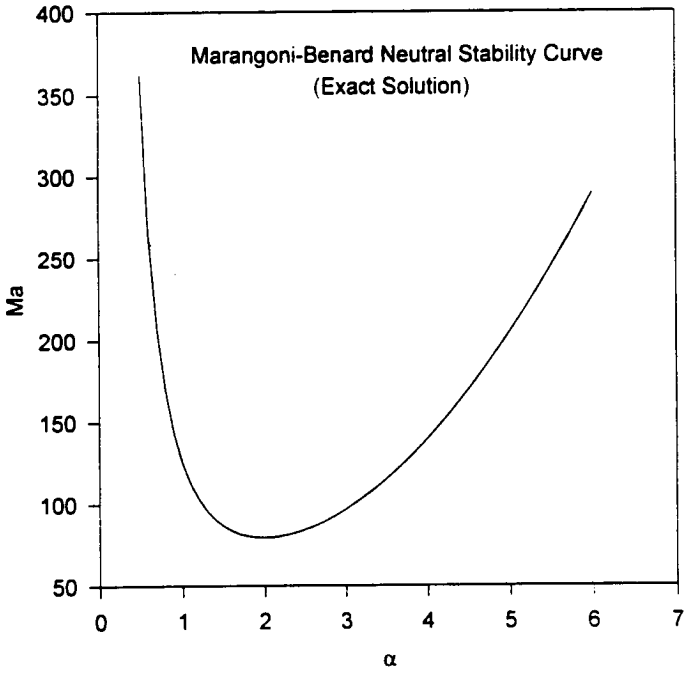

Figure 2 Marangoni-Benard Neutral Stability Curve, Exact Solution for Bi=0 (Pearson, 1958)

Neutral stability curves for the Marangoni-Benard problem which were generated using a 2nd order finite difference scheme and spectral scheme are shown in Figs. 3 and 4, respectively. The number of points across the fluid depth, N, (in the z-direction) represents the spatial resolution used to generate a given curve. In Fig. 3 the neutral stability curve converges to the exact solution as the spatial resolution increases from N = 4 to N = 100. The N = 50 and N = 100 curves are visually indistinguishable from the exact solution. Fig. 4 reveals that the neutral stability curves computed using the spectral formulation also converge to the exact solution as the spatial resolution increases. The spectrally generated neutral stability curves shown in Fig. 4 are visually identical to the exact solution for spatial resolutions as low as N = 10. In both Figs. 3 and 4, the numerically generated neutral stability curves tend to diverge from the exact solution with increasing wavenumber. It is also observed that the finite difference solution converges from above the exact solution while the spectral solution converges from below exact neutral stability curve.

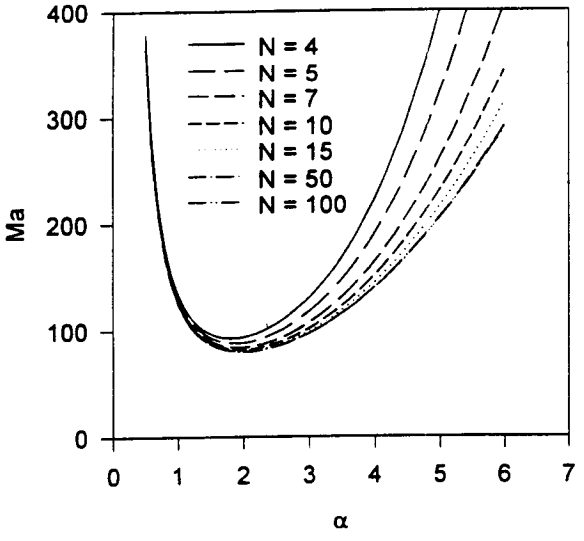

Figure 3 Marangoni-Benard Neutral Stability Curves Computed Using A 2nd Order Finite Difference Scheme. N Is The Number Points Through The Fluid Layer.

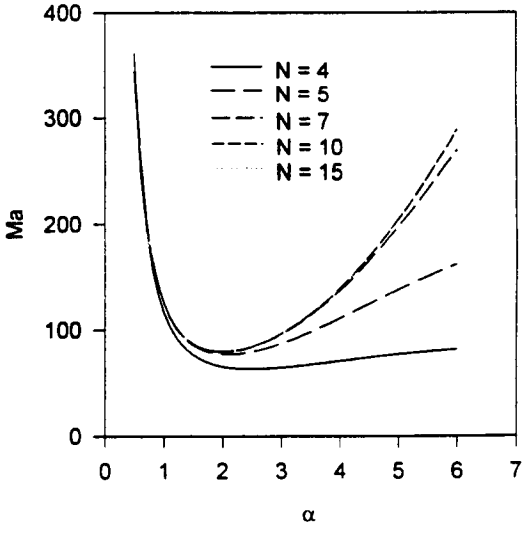

Figure 4 Marangoni Neutral Stability Curves Computed Using A Spectral Collocation Scheme. N The Number Points Through The Fluid Layer.

The error in the Marangoni number for the finite difference and spectral schemes is plotted as a function of wavenumber in Figs. 5 and 6, respectively. In both figures, error is plotted using a logarithmic scale while the wavenumber. α, is plotted with a linear scale on the abscissa. The error (ordinate) range differs between the two figures so that the error characteristics of each discrete scheme could be observed. The error is defined as $\frac{Ma_N - Ma_{exact}}{Ma_{exact}}$ where Ma_N is the Marangoni number computed from a discrete formulation for a given spatial resolution (N points) and Ma_{exact} is computed using equation (35). Both discrete schemes are observed in Figs. 1 through 4 to converge to the exact solution as the spatial resolution, N, increases. The finite difference errors for each

curve increase approximately an order of magnitude over the given wavenumber range as observed in Figure 5, while the spectral error shown in Figure 6 increases four to five orders of magnitude with wavenumber. For N greater than approximately seven. the spectral error remains considerably less than the finite difference error for the range of α considered.

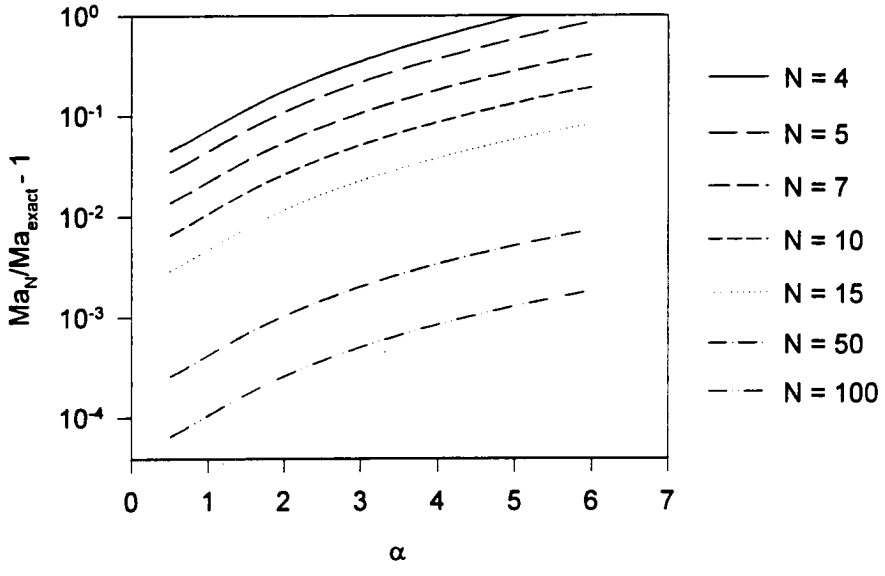

Figure 5 Marangoni Number Error vs. Wavenumber For The 2nd Order Finite Difference Solution. N Is The Number Of Points Through The Fluid Layer

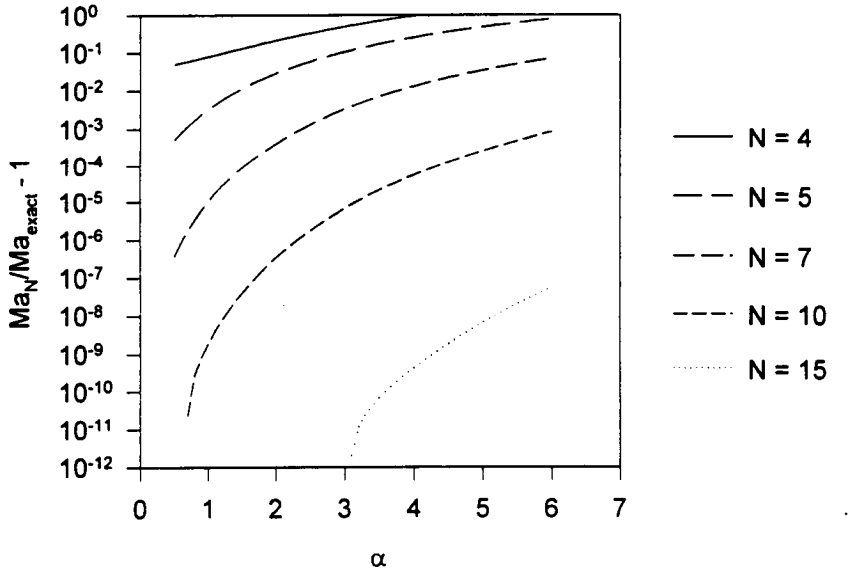

Figure 6 Marangoni Number Error vs. Wavenumber For The Spectral Collocation Scheme. N Is The Number Of Points Through The Fluid Layer

Selected error values of the two schemes for wavenumbers of 2 and 5 are tabulated in Tables 1 and 2, respectively. The errors for , $\alpha = 2$, the critical wavenumber were smaller than those of the larger wavenumber, $\alpha = 5$. In Fig. 7, the Ma error is shown on a log-log plot as function of the spatial resolution (N grid points) for both discrete formulations . Comparing Ma error values at a wavenumber of 2 and N = 10, the error for the spectral scheme is seen to be five orders of magnitude smaller than the finite difference error. Furthermore, after increasing the spatial resolution of the finite difference scheme to N = 100, still gives a spectral error **for N = 10** that is 3 orders of magnitude smaller. The reduction in error for the finite difference scheme is essentially proportional to N^2, as expected since the scheme is 2^{nd} order accurate. A slope of -2.02 was computed for the finite difference curve in Fig. 7 which is within 1% of the expected value of 2. The slope was computed from a least squares fit of the finite difference data in Table 1. The error for the spectral formulation is expected to decrease exponentially with increasing N (Boyd, 1989, Canuto et. al., 1987). However the error results in Table 2 show that the exponential rate of convergence is exceeded for this particular problem. Fig. 7 vividly illustrates that the spectral scheme results in a significant reduction in error with considerably fewer grid points than the central difference scheme for this particular problem. The spectral formulation has also been shown to out perform finite difference methods when applied to other hydrodynamic stability problems (Canuto et. al., 1987, Boyd, 1989). The exceptional performance (greater than exponential convergence) of the spectral collocation scheme for this problem was not anticipated by the authors.

Table 1 Selected Marangoni Number Errors For Wavenumber, α=2

Spatial resolution N	Finite Difference	Spectral
5	1.085×10^{-1}	2.920×10^{-2}
10	2.600×10^{-2}	3.400×10^{-7}
15	1.115×10^{-2}	4.529×10^{-11}
50	1.025×10^{-3}	
100	2.561×10^{-4}	

Table 2 Selected Marangoni Number Errors For Wavenumber, α=5

Spatial resolution N	Finite Difference	Spectral
5	5.756×10^{-1}	2.808×10^{-1}
10	1.309×10^{-1}	2.525×10^{-4}
15	5.710×10^{-2}	6.434×10^{-9}
50	5.075×10^{-3}	
100	1.268×10^{-3}	

As stated throughout, the ability to reduce the size of N is crucial to the eigenvalue problem, $A\bar{x} = \lambda B\bar{x}$. Inverting B takes $O(N^3)$ operations; the matrix multiplication of $C = B^{-1}A$ requires $O(N^3)$; and solving the regular eigenvalue problem, $C\bar{x} = \lambda\bar{x}$, requires $O(N^3)$ operations. Neglecting all other operations than those identified above, for a grid resolution of N=10, it requires appropriately 3000 operations to compute the eigenvalues while it requires $O(3 \times 10^6)$ operations for N=100. The number of iterations required to converge to Ma_c at one wavenumber is O(10), ie., the matrix eigenvalue problem is solved approximately ten times for each wavenumber.

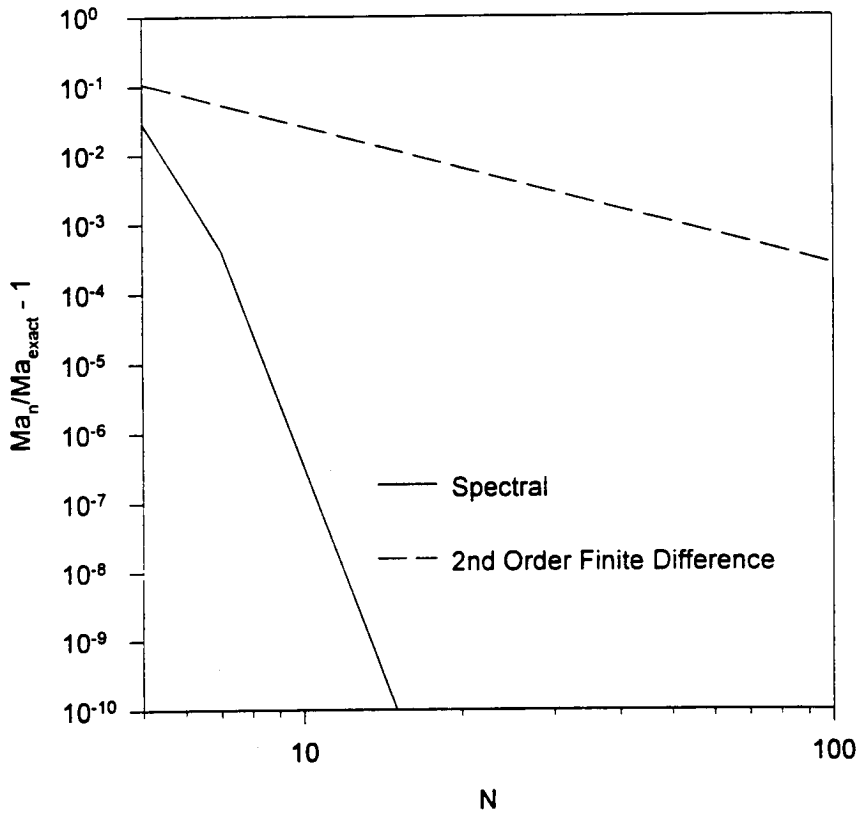

Figure 7 Error in Ma_c ($\alpha = 2$) As A Function Of The Number of Points Across The Fluid Layer, N

5.0 Concluding Remarks

A spectral scheme, the Chebyshev collocation formulation was used to perform a hydrodynamic (linear) stability analysis of the Benard problem. The problem reduces to a generalized eigenvalue problem, $Ax = \lambda Bx$, which can be reduced to a regular eigenvalue problem, $Cx = \lambda x$ by inverting B. Implementation of the spectral scheme was described. There is a bit of a learning curve that must initially be overcome to comfortably setup the spectral formulation if one has no previous experience with spectral methods. Afterwards, the spectral scheme requires only slightly more time to set up than the 2nd order finite difference scheme and is likely to be easier to program than higher order finite difference schemes. A comparison of the results from the spectral and finite difference scheme reveals that the spectral scheme out performs the finite difference scheme by a considerable margin. The error of the spectral scheme is at least three orders of magnitude smaller than the finite difference error for $N = 10$ and seven orders of magnitude smaller than finite difference error for $N = 15$.

6.0 References

Adamson, A.W., Physical Chemistry of Surfaces, John Wiley & Son's, 1967.

Boyd, J. P., Chebyshev & Fourier Spectral Methods, Springer-Verlag, New York, 1989.

Chandrasekhar, S., Hydrodynamic and Hydromagnetic Stability, Dover, New York, 1981.

Canuto, C., and M. Y. Hussaini, A. Quarteeroni, and T.A. Zang, Spectral Methods in Fluid Dynamics, Springer-Verlag, New York, 1987.

Drazin, P.G., and W.H. Reid, Hydrodynamic Stability, Cambridge University Press, 1991.

Incropera, F. P., and D. P. DeWitt, Fundamentals of Heat and Mass Transfer, John Wiley and Sons, New York, 1985.

Koschmieder, E.L., Benard Cells and Taylor Vortices, Cambridge University Press, 1993.

Legros, J.C., O. Dupont, P. Queeckers, S. Van Vaerenbergh, and D. Schwabe, "Thermohydrodynamic Instabilities and Capillary Flow," Low Gravity Fluid Dynamics and Transport Phenomena, Ed J. Koster and R. Sani, American Institute of Aeronautics and Astronautics, 1990.

Lin, C.C., The Theory of Hydrodynamic Stability, Cambridge University Press, New York, 1966

Nield, D. A., "Surface Tension and Buoyancy Effects In Cellular Convection," Journal of Fluid Mechanics, Vol. 19, 1964, pp. 341-352.

Ostrach, S., "Low-Gravity Fluid Flows," Annual Review of Fluid Mechanics, Vol 14, 1982, pp. 313-345.

Pearson, J. R. A., "On Convection Cells Induced by Surface Tension," Journal Of Fluid Mechanics, Vol. 4, 1958, pp. 489-500.

Scriven, L. E., and C. V. Sternling, "On Cellular Convection Driven By Surface-Tension Gradients: Effects Of Mean Surface Tension and Surface Viscosity," Journal Of Fluid Mechanics, Vol. 19, 1964, pp. 321-340.

Smith, K. A., "On Convective Instability Induced By Surface Tension Gradients," Journal Of Fluid Mechanics, Vol 24, 1966, pp. 401-414.

"Microgravity Science and Applications: Program Tasks and Bibliography for FY 1993," NASA TM-4569, March 1994.